Petrogenesis of Plio-Quaternary basanites in the Gandom Beryan area, Kerman,Iran: geochemical evidence for the low-degree partial melting of enriched mantle

SEYED JAVAD YOUSEFI

ABBAS MORADIAN

HAMID AHMADIPOUR

Petrogenesis of Plio-Quaternary basanites in the Gandom Beryan area, Kerman, Iran: geochemical evidence for the low-degree partial melting of enriched mantle

Seyed Javad YOUSEFI, Abbas MORADIAN*, Hamid AHMADIPOUR
Department of Geology, Faculty of Sciences, Shahid Bahonar University, Kerman, Iran

Abstract: In the Gandom Beryan area, basanitic lava flows erupted from fractures in the Nayband fault zone and formed an area of about 300 km² of basanitic rocks in the western part of the Lut Block. Olivine and clinopyroxene are the major phenocrysts in a microlitic groundmass for these basanitic rocks. The geochemical data show that Gandom Beryan rocks are basanite in composition and belong to intercontinental rifts related to alkali basanites. These rocks have low Fe/Mg ratios (Fe_2O_{3t}/MgO = 1.07–1.43) with low silica content (SiO_2 = 44.89–48.26 wt.%) and are high-Ti basanites. The investigated rocks are characterized by a significant enrichment of total REE and LREE relative to chondrite. Moreover, the REE patterns of these rocks are linear without any negative Eu anomalies. The low abundances of HREE in basanitic rocks and the REE modeling together reflect the relation between these elements and residual garnet in the partially melted mantle. The $^{207}Pb/^{204}Pb$ and $^{206}Pb/^{204}Pb$ ratios of the basanitic rocks fall near the field of enriched mantle II (EM-II). The Gandom Beryan volcanism, which was related to partial melting of mantle within an extensional setting, resulted from a left-step, pull-apart basin in the Nayband N–S trending strike–slip fault system. Although the fault system is older than Gandom Beryan volcanism, it seems that it has been reactivated during and after the volcanism.

Key words: Lut Block, Gandom Beryan area, basanite, Geochemistry, Nd-Sr-Pb isotopes

1. Introduction

The composition and origin of continental intraplate basaltic volcanism including that of small volcanic fields and enormous flood basalt provinces have received significant attention over the past few decades. Some of the continental intraplate basaltic eruptions are directly related to heterogeneous sources that exist in the shallow mantle (e.g., Meibom and Anderson, 2003; Aldanmaz et al., 2006) or in the lithospheric mantle (e.g., Hawkesworth et al., 1992; Späth et al., 2001; Weinstein et al., 2006; Ma et al., 2011b). The degrees of partial melting and fractional crystallization control the geochemical and isotopic compositions of such basalts (e.g., Peters et al., 2008). Moreover, the continental intraplate basalts have different compositions, which is indicative of variations in their mantle source regions (O'Reilly and Zhang, 1995; Xu et al., 2005; Tang et al., 2006; Niu, 2008) and/or to crustal contamination (Carlson et al., 1981; Mahoney, 1988; Koszowska et al., 2007; Rocha-Júnior et al., 2013) during magma ascent.

The Gandom Beryan area is located on the western margin of the Lut Block (LB), along the Nayband fault (Figure 1). There are no towns/cities/villages in the mapped area; the nearest towns to the study area are

Shahdad (about 70 km to the south) and Ravar (about 85 km to the west).

The basanitic lavas erupted from fractures of the Nayband fault zone and covered an area of about 300 km² of basanitic rocks. The occurrence and origin of basanites in Gandom Beryan were poorly documented by Stöcklin et al. (1971), Samani et al. (1994), Walker et al. (2009), and Raeisi (2011). Walker et al. (2009) investigated active faulting in the area and carried out $^{40}Ar/^{39}Ar$ age dating and geochemistry of volcanic rock exposed along the Nayband fault zone in the Gandom Beryan area. Based on the limited dataset of major and trace elements, the geochemistry of the southeast of the Gandom Beryan area was studied by Raeisi (2011). Therefore, systematic geochemistry and isotopic studies of these basanites are necessary to investigate igneous occurrences and petrogenesis of Gandom Beryan basanites.

In this study, we report mineral, whole rock chemistry, and Nd, Sr, and Pb isotopic compositions for basanitic rocks of the Gandom Beryan area in the western LB. The purpose of this study is to reveal geochemical and isotopic features of these basanites in order to clarify the genesis and petrological evolutions of the magma source areas.

---

* Correspondence: moradian@uk.ac.ir
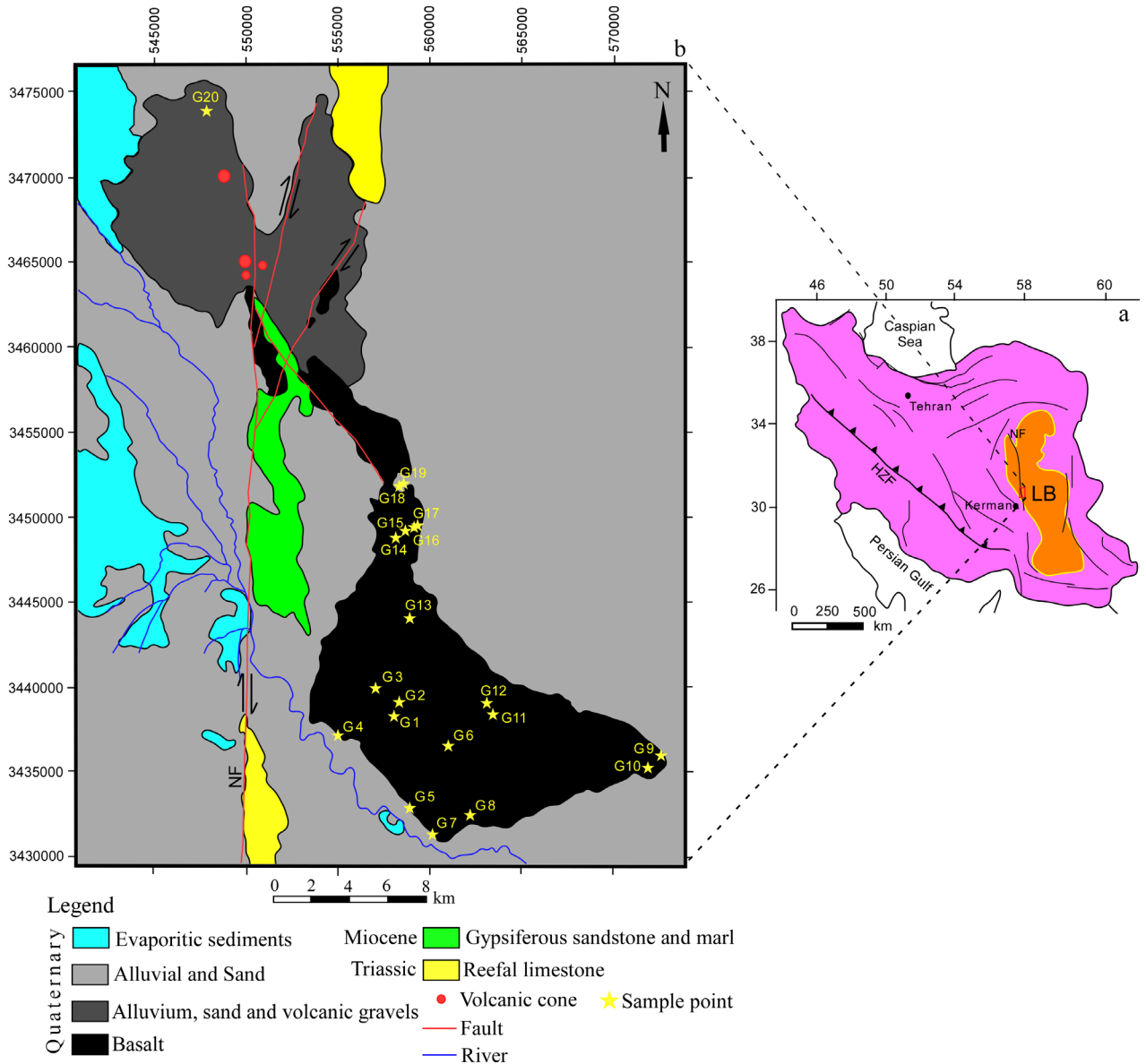
Figure 1. a. Modified geological map of Iran, showing the location of the major faults, Lut Block (LB), Nayband fault (NF), and study area (after Berberian and King, 1981), b. Geological map of Gadom Beryan area, adapted from Kluyver et al. (1981). HZF (High Zagros Fault).

2. Geological setting

The LB is located in eastern Iran. It is applied to the north trending desert belt, which is 700 km long with an average width of 150–200 km (Figure 1a). The basement of the LB is represented by metamorphic rocks that have not been dated (Saadat et al., 2010). Marine carbonate, sandstone, and shale are the major sedimentary strata in the LB that are younger than Permian (Stöcklin et al., 1971). Magmatism in the LB started in the Late Jurassic period and continued to the Quaternary to form a variety of volcanic, subvolcanic, and intrusive rocks (Esmaiely et al., 2005; Saadat et al., 2010). The basement and its sedimentary cover were invaded by

several Mesozoic and Tertiary dioritic and granitic intrusive bodies (Stöcklin et al., 1971). The LB has a simple structure, dominated by gentle folding, faulting in different directions, and tilting (Stöcklin et al., 1971).

The Gandom Beryan area is located in the western part of the LB (Figure 1). Triassic reefal limestones are the oldest stratum, exposed in the north and southwest of the Gandom Beryan area (Figure 1b). There are extremely abundant algae and less common corals, crinoids, and lamellibranchs in this unit. Moreover, dolomitization occurred locally in this limestone. Gypsiferous sandstone and marl unit of Miocene have outcrops in the central

285

part of this area (Figure 1b). This unit is formed from the alternation of gypsiferous sandstone and marl (Kluyver et al., 1981).

The Plio-Quaternary basanitic rocks that are the main subject of our research extended from the center to the southeast of the study area (Figure 1b). Based on ^{40}Ar/^{39}Ar age dating by Walker et al. (2009), these rocks are in 2.20–2.60 million years of age. According to Walker et al. (2009), Gandom Beryan basanitic lava flows erupted from volcanic cones along the faults. The huge accumulation of alkali basanitic lavas flowed towards the south and southeast of the eruptive cones and formed the Gandom Beryan basanitic rocks. The eruptive cones are placed near a left-step, pull-apart basin (about 10-km long and 5-km wide) in the Nayband fault (Walker et al., 2009). Local extension inside the pull-apart basin might have affected the volcanism situation (e.g., Camp and Griffis, 1982). Neogene-Quaternary continental sedimentary deposits are the youngest geological stratum in the LB.

3. Field characteristics
Field studies show that the basanitic rocks of Gandom Beryan occur along the Nayband N–S trending strike–slip fault. Nabavi (1976) attributed this fault to the Katangan fault systems, and showed that the southern part of this fault raised Paleogene dacitic magmas. In addition, Walker and Jackson (2002) argued that the Gandom Beryan basanites postdate the initiation of the Nayband fault. Therefore, it seems that this part of the Nayband fault was reactivated during and after the formation of Gandom Beryan basanites. Furthermore, lavas have flowed on marine sedimentary deposits. The lava flows caused baking of underlying Neogene-Quaternary sedimentary deposits

and changed their colors (Figure 2). The thicknesses of basanitic rocks vary from 1 to 10 m. The aphanitic and vesicular structures are the most important features in the basanites. Vesicles have circular and ellipsoidal shapes that indicate the degassing of volatiles from lava. These vesicles were filled with secondary minerals such as gypsum.

4. Petrography
Gandom Beryan basanitic rocks have porphyritic, microlitic, glomeroporphyritic, intergranular, and vesicular textures (Figure 3). According to Mackenzie et al. (1982), phenocrysts range from 2 to 5 mm in size, microphenocrysts sizes range from 1 to 2 mm, and the size of microlites is <1 mm. Gandom Beryan basanites have anhedral, subhedral, and euhedral olivine phenocrysts up to 3 mm in diameter that consist of 3–5 vol. % of the rocks, while olivine microphenocrysts and fine-grained euhedral olivine consist of 10–15 and about 5 vol. % of the rocks, respectively. Some olivine phenocrysts show embayment corrosions, probably due to the disequilibrium conditions or crystal fractionation resorption (Figure 3f). Some olivines converted to iddingsite. Clinopyroxene phenocrysts with up to 4.5 mm in diameter include 5–8 vol. % of the rocks and some of them exhibit zoning texture (Figure 3b). Microphenocrysts and fine-grained clinopyroxene comprise 8–10 vol. % of the basanites as well. Clinopyroxene slightly converted to chlorite. Microlitic plagioclases consist of more than 55 vol % of the rocks, which together with fine-grained olivine and clinopyroxene, formed the groundmass of the basanites. Plagioclase microlites display albite twinning and are slightly weathered. As accessory minerals, apatite and opaque include less than 1 vol. % of the rocks.
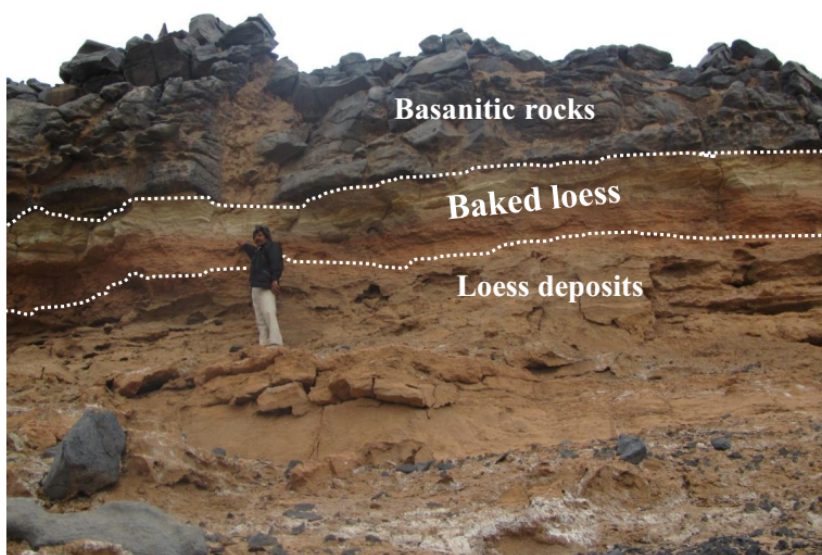
Figure 2. The heat of basanitic lava flows has been baked the underlying loess deposits and changed their color in the southern part of the Gandom Beryan area.
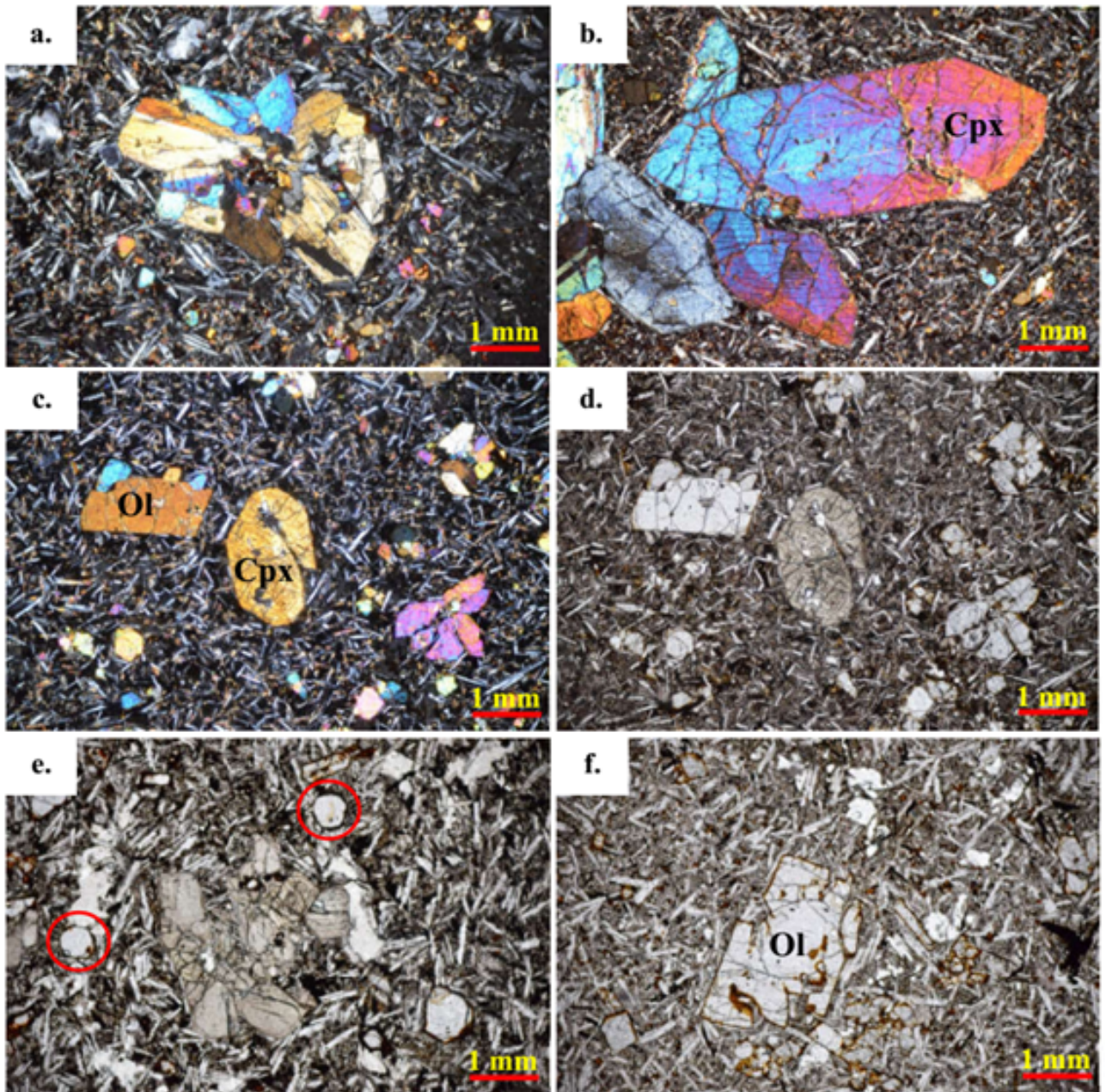
Figure 3. a. Photomicrograph (XPL) of glomeroporphyritic texture contains clinopyroxene phenocrysts clusters, b. Photomicrograph (XPL) of basalt shows zoned clinopyroxene phenocrysts, c. Photomicrograph (XPL) of the studied basalt contains microlitic plagioclases (white color), small olivine and clinopyroxene in groundmass, d. Polarized light image of Figure 3. c, e. Rounded olivines in the studied basalt shown with red circles, f. Photomicrograph (PPL) of the studied basalt and a subhedral olivine displaying the magmatic corrosion.

5. Analytical techniques

The chemical analyses of the minerals were conducted using a Cameca SX-100 electron microprobe with ZAF matrix correction at Iran Minerals Production and Supply Company (IMPASCo). The machine was operated with an electron gun accelerating voltage of 15 kV (15 s background counting times), beam current of 20 nA, and 3 μm diameter of focused beam. All the chemical compositions of the minerals presented here indicate the average of the three analytical objects of each mineral.

Petrographic studies were carried out on 120 samples and 20 relatively fresh samples were chosen for the whole rock geochemical analyses. X-ray fluorescence (XRF) spectrometry was applied to analyze major element oxides. In addition, the trace elements were analyzed using inductivity coupled plasma mass spectrometry followed by

lithium borate fusion and dilute acid digestion. Both the XRF and ICP-MS analyses were carried out in the ACME laboratories, Vancouver, Canada.

Pb, Nd, and Sr isotopic compositions were analyzed for six whole rock samples of the Gandom Beryan basanitic rocks at the ACME laboratories, Vancouver, Canada. For sample digestion 200–400 mg of rock powder was dissolved using hydrofluoric, nitric, and hydrochloric acids. Sr was purified using cation exchange resin with 2.5 N HCl. Sr was loaded onto pre-outgassed and clean rhenium filaments with phosphoric acid and tantalum oxide. Sr isotopes were analyzed using thermal ionization mass spectrometry (TIMS) and five Faraday collectors in dynamic mode and $^{88}Sr = 3.0$ V. Sr isotopes were normalized to $^{86}Sr/^{88}Sr = 01194$ and corrected for any Rb present during the analysis. Nd was purified using HDHEP coated resin and 0.25 N HCl. Nd isotopes were analyzed, using MC-ICPMS, with seven Faraday collectors and dissolved in 2% HNO_3. Nd isotopes

were normalized to $^{146}Nd/^{144}Nd = 0.7219$ and corrected for any Sm during analysis. All analyses were undertaken using a spray chamber. Pb was purified using anion exchange resin and 1 N HBr. Pb isotopes were analyzed using MC-ICPMS with five Faraday collectors and with samples dissolved in 2% HNO_3. Samples were doped with NBS997 Tl with Pb/Tl ratios of ≤2 and Pb isotopes were normalized to $^{203}Tl/^{205}Tl = 0.41892$. All analyses were undertaken using a spray chamber. NBS987 Standard Sr was analyzed for Sr; also JNdi-1 was analyzed for Nd and NBS981 Standard was analyzed for Pb. None of the results were normalized to standard results.

6. Results

6.1. Mineral chemistry
Representative chemical compositions of the olivines and clinopyroxene are reported in Table 1. Totally more than 27, 18, and 6 microprobe point analyses were performed

Table 1. Representative chemical analyses of olivine and clinopyroxene from Gandom Beryan basalts.

	Unit	Standard materials	Olivine			Clinopyroxene		
			G-Ol-1	G-Ol-2	G-Ol-3	G-Cpx-1	G-Cpx-2	G-Cpx-3
SiO_2	wt.%	Wollastonite	38.92	40.73	39.18	47.99	43.51	47.49
TiO_2	wt.%	Rutile	0	0	0	2.08	4.54	3.07
Al_2O_3	wt.%	Corundum	0.3	0	1.32	4.55	8.69	6.46
Cr_2O_3	wt.%	Chromite	0.03	0.02	0.06	0.0	0.01	0.0
Fe_2O_3	wt.%	Specularite	16.65	14.94	20.09	6.14	8.1	5.52
MnO	wt.%	Rhodonite	0.25	0.17	0.24	0.11	0.08	0.14
MgO	wt.%	Periclase	42.89	43.31	38.42	13.52	10.8	11.68
CaO	wt.%	Wollastonite	0.25	0.08	0.23	22.41	21.07	22.54
Na_2O	wt.%	Albite	0	0	0	0.53	0.73	0.66
Total	wt.%		99.29	99.25	99.54	97.33	97.59	97.56
Si			1.0	1.03	1.02	1.82	1.67	1.809
Ti			0	0	0	0.06	0.13	0.088
Al			0.009	0	0.04	0.204	0.393	0.290
Cr			0.001	0	0.001	0.0	0.00	0.00
Fe			0.32	0.28	0.39	0.12	0.197	0.176
Mn			0.005	0.004	0.005	0.004	0.003	0.005
Mg			1.65	1.64	1.49	0.76	0.618	0.66
Ca			0.007	0.002	0.006	0.912	0.86	0.92
Na			0	0	0	0.039	0.058	0.049
Fo			83.39	85.01	78.90	-	-	-
Fa			16.34	14.80	20.82	-	-	-
Tp			0.27	0.19	0.28	-	-	-
Wo			-	-	-	50.65	41.53	52.30
En			-	-	-	42.52	36.75	37.71
Fs			-	-	-	6.83	11.71	10.00
Mg#			83.61	88.59	79.12	86.15	75.83	78.95

for olivine, clinopyroxene, and plagioclase, respectively. The olivine ranges in composition from $Fo_{78.9}$ to $Fo_{85.01}$ with Mg number [Mg# = $100 \times$ Mg/(Mg + Fe_{total})] ranging from 79.12 to 88.59. Clinopyroxenes are diopsitic in composition ($Wo_{41.53–52.30}$ $En_{36.75–42.52}$ $Fs_{6.83–11.71}$) with Mg number ranging from 75.83 to 86.15. The TiO_2 and Al_2O_3 compositions of the clinopyroxenes vary from 2.08 to 4.54 and from 4.55 to 8.69 wt.%, respectively.

6.2. Whole-rock chemistry

The whole-rock major and trace element data with their Mg numbers are given in Table 2. The samples G10 and G11 were neglected because of high LOI. On the basis of the total

Table 2. Whole rock geochemical analyses of the Gandom Beryan basanitic rocks.

	Unit	MDL	G1	G2	G3	G4	G5	G6	G7	G8	G9	G10
SiO_2	wt.%	0.01	46.02	47.68	46.75	46.15	46.77	47.30	47.41	48.26	46.18	45.32
Al_2O_3	wt.%	0.01	13.27	13.61	13.41	13.15	13.43	13.69	13.44	13.71	13.38	12.96
Fe_2O_3	wt.%	0.04	10.74	11.00	10.79	10.86	11.04	10.94	10.88	10.98	10.84	10.66
MgO	wt.%	0.01	7.99	7.80	7.88	8.12	8.15	8.08	7.86	7.73	7.90	8.27
CaO	wt.%	0.01	9.21	7.71	8.32	9.04	8.88	8.19	7.80	7.55	8.09	7.99
Na_2O	wt.%	0.01	4.68	3.95	4.16	4.40	4.12	4.06	4.16	3.98	4.42	5.04
K_2O	wt.%	0.01	2.17	2.74	2.33	2.08	2.57	2.82	2.69	2.73	2.44	2.60
TiO_2	wt.%	0.01	2.35	2.64	2.39	2.30	2.34	2.34	2.62	2.69	2.37	2.28
P_2O_5	wt.%	0.01	0.87	0.83	0.89	0.90	0.94	0.92	0.81	0.81	0.92	0.86
MnO	wt.%	0.01	0.15	0.14	0.15	0.15	0.15	0.15	0.14	0.14	0.15	0.15
Cr_2O_3	wt.%	0.002	0.028	0.029	0.028	0.029	0.029	0.028	0.029	0.028	0.027	0.029
Ni	ppm	20	103	131	107	119	123	119	133	137	112	117
Sc	ppm	1	16	15	16	17	17	16	15	15	16	16
LOI	wt.%	-5.1	2.1	1.5	2.5	2.4	1.1	1.0	1.7	1.0	2.9	3.4
Sum	wt.%	0.01	99.55	99.59	99.57	99.56	99.56	99.57	99.59	99.60	99.59	99.58
Ba	ppm	1	560	516	557	574	567	575	493	540	565	550
Be	ppm	1	1	3	5	3	1	3	1	2	1	2
Co	ppm	0.2	46.7	43.0	42.5	46.1	42.4	47.0	44.7	44.9	42.8	45.9
Cs	ppm	0.1	0.9	0.8	0.7	1.0	0.7	1.1	0.7	0.7	0.8	0.6
Ga	ppm	0.5	19.7	19.9	19.9	19.2	18.7	19.4	20.5	20.7	18.9	19.1
Hf	ppm	0.1	4.9	4.6	4.5	4.9	5.1	4.9	4.9	4.8	4.6	4.6
Nb	ppm	0.1	72.5	70.9	74.0	73.3	72.1	75.6	68.9	72.3	74.6	71.9
Rb	ppm	0.1	46.2	47.6	25.7	43.9	42.5	48.6	45.3	48.6	34.3	47.0
Sn	ppm	1	2	2	2	2	2	2	2	2	2	2
Sr	ppm	0.5	1100.6	913.9	948.4	1027.6	1009.7	976.4	910.1	828.8	881.9	915.6
Ta	ppm	0.1	3.6	3.9	3.8	3.4	3.8	3.9	3.4	3.6	4.0	3.7
Th	ppm	0.2	6.5	5.2	6.1	6.2	6.8	6.7	5.0	5.9	6.5	6.4
U	ppm	0.1	1.5	0.4	0.7	1.5	1.4	1.0	0.6	0.6	1.3	1.5
V	ppm	8	176	182	181	176	178	172	178	176	175	173
W	ppm	0.5	2.0	1.3	1.5	1.8	1.7	1.7	1.0	0.8	1.2	1.2
Zr	ppm	0.1	215.0	214.6	206.6	210.8	207.5	213.1	208.9	209.6	202.9	205.4
Y	ppm	0.1	21.6	20.6	22.9	22.1	22.1	23.3	19.6	21.2	20.7	21.8
La	ppm	0.1	47.0	40.5	50.7	50.8	53.2	51.5	45.6	44.0	54.3	52.2
Ce	ppm	0.1	87.8	79.8	86.8	92.4	94.3	91.5	84.2	84.9	93.3	94.0
Pr	ppm	0.02	10.57	9.59	10.67	11.08	11.77	11.23	9.83	9.65	10.93	10.96
Nd	ppm	0.3	40.8	39.0	41.6	41.9	42.6	42.9	39.3	39.6	41.9	41.4
Sm	ppm	0.05	7.65	7.25	7.59	7.52	7.91	7.78	7.21	7.22	7.90	7.76
Eu	ppm	0.02	2.39	2.31	2.35	2.50	2.58	2.47	2.43	2.36	2.32	2.48
Gd	ppm	0.05	6.96	6.27	6.96	7.02	7.26	7.30	6.80	6.41	7.10	6.74
Tb	ppm	0.01	0.90	0.89	0.95	0.94	0.97	0.99	0.90	0.89	0.97	0.94
Dy	ppm	0.05	4.93	4.60	4.68	4.56	4.92	4.93	4.77	4.41	5.03	4.70
Ho	ppm	0.02	0.76	0.73	0.76	0.80	0.83	0.79	0.72	0.76	0.80	0.81
Er	ppm	0.03	1.84	1.95	1.94	2.09	2.28	2.10	1.96	2.02	1.95	1.85
Tm	ppm	0.01	0.27	0.27	0.25	0.26	0.27	0.28	0.25	0.24	0.25	0.25
Yb	ppm	0.05	1.68	1.45	1.61	1.67	1.54	1.74	1.54	1.47	1.63	1.58
Lu	ppm	0.01	0.22	0.21	0.21	0.22	0.25	0.25	0.21	0.22	0.23	0.22
TOT/C	wt.%	0.02	0.09	0.06	0.13	0.13	0.11	0.06	0.05	0.12	0.10	0.05
TOT/S	wt.%	0.02	0.69	0.12	0.07	0.23	0.18	0.08	0.05	0.05	0.03	0.06
Mg#			59.58	58.42	59.13	59.70	59.39	59.40	58.87	58.24	59.08	-

Table 2. (Continued).

|	Unit	MDL	G11	G12	G13	G14	G15	G16	G17	G18	G19	G20
SiO_2	wt.%	0.01	46.77	48.10	47.13	48.05	47.87	47.79	47.26	46.03	46.90	44.89
Al_2O_3	wt.%	0.01	15.88	13.57	13.55	13.63	13.64	13.62	13.47	13.35	13.36	12.78
Fe_2O_3	wt.%	0.04	9.94	11.20	10.71	10.97	10.90	10.91	10.89	10.69	10.82	11.06
MgO	wt.%	0.01	3.43	7.81	7.72	7.90	7.78	8.02	8.11	7.86	8.03	10.29
CaO	wt.%	0.01	7.28	7.31	8.17	8.02	7.98	7.98	7.96	8.29	8.04	9.05
Na_2O	wt.%	0.01	5.17	4.06	4.42	4.03	3.84	3.91	4.54	5.04	3.85	4.56
K_2O	wt.%	0.01	3.44	2.60	2.32	2.74	2.78	2.74	2.34	2.28	2.79	2.81
TiO_2	wt.%	0.01	2.70	2.81	2.52	2.53	2.55	2.50	2.45	2.39	2.42	2.37
P_2O_5	wt.%	0.01	1.18	0.82	0.85	0.85	0.85	0.84	0.89	0.88	0.91	1.43
MnO	wt.%	0.01	0.13	0.14	0.14	0.15	0.14	0.14	0.15	0.14	0.15	0.16
Cr_2O_3	wt.%	0.002	<0.002	0.028	0.029	0.028	0.029	0.028	0.029	0.028	0.029	0.054
Ni	ppm	20	23	136	116	117	119	120	106	104	107	237
Sc	ppm	1	9	14	15	16	16	16	16	16	16	16
LOI	wt.%	-5.1	3.7	1.1	2.0	0.7	1.2	1.1	1.5	2.6	2.3	-0.1
Sum	wt.%	0.01	99.60	99.59	99.59	99.59	99.60	99.59	99.59	99.59	99.59	99.36
Ba	ppm	1	732	550	507	527	507	507	552	547	525	1101
Be	ppm	1	4	1	2	5	2	4	2	4	3	5
Co	ppm	0.2	28.5	45.4	42.3	44.8	41.5	42.3	44.0	42.4	43.7	45.1
Cs	ppm	0.1	1.0	0.8	0.7	0.5	0.7	0.4	1.1	0.7	0.9	0.8
Ga	ppm	0.5	21.8	20.3	20.3	20.2	20.4	20.9	19.6	19.1	19.2	18.6
Hf	ppm	0.1	6.1	5.0	4.9	5.2	5.4	5.1	4.9	4.9	5.0	5.6
Nb	ppm	0.1	95.9	74.8	71.4	71.7	69.5	69.8	74.1	70.2	71.4	142.6
Rb	ppm	0.1	49.9	51.9	46.0	45.4	48.5	47.2	42.1	43.4	48.2	48.3
Sn	ppm	1	2	2	2	2	2	2	2	2	2	2
Sr	ppm	0.5	1066.4	839.4	904.0	862.4	839.2	874.3	890.2	882.3	861.1	1610.6
Ta	ppm	0.1	5.2	3.8	3.7	4.0	3.6	3.7	3.9	3.7	3.7	6.4
Th	ppm	0.2	8.0	5.1	5.4	5.8	5.6	5.6	5.9	5.9	5.5	10.7
U	ppm	0.1	1.8	0.5	1.6	1.3	0.8	0.9	1.4	1.4	1.2	2.4
V	ppm	8	164	170	176	180	185	177	174	171	178	157
W	ppm	0.5	1.0	0.8	1.6	0.7	1.7	0.7	1.0	1.1	1.3	1.5
Zr	ppm	0.1	232.9	210.8	213.4	216.0	205.6	203.9	213.0	206.8	199.2	276.2
Y	ppm	0.1	25.4	20.7	21.8	20.5	21.0	22.2	22.1	21.9	21.5	24.1
La	ppm	0.1	69.9	44.0	43.9	44.0	46.4	46.3	49.9	47.5	49.2	96.8
Ce	ppm	0.1	119.0	81.8	79.6	81.1	82.0	82.5	84.1	86.6	87.1	171.2
Pr	ppm	0.02	14.05	9.77	9.53	9.92	9.90	10.02	10.19	10.07	10.24	20.32
Nd	ppm	0.3	53.8	39.5	40.4	37.5	38.9	37.1	42.0	40.9	40.5	74.9
Sm	ppm	0.05	9.36	7.35	7.33	7.29	7.02	7.35	7.43	7.21	7.43	11.62
Eu	ppm	0.02	2.87	2.45	2.39	2.41	2.27	2.39	2.52	2.22	2.38	3.39
Gd	ppm	0.05	8.21	6.58	6.88	6.66	6.53	6.78	6.83	6.74	6.59	9.02
Tb	ppm	0.01	1.08	0.89	0.89	0.90	0.90	0.91	0.92	0.85	0.90	1.12
Dy	ppm	0.05	5.33	4.68	4.63	4.48	4.67	4.71	4.80	4.48	4.75	5.48
Ho	ppm	0.02	0.90	0.72	0.74	0.75	0.72	0.79	0.79	0.71	0.77	0.86
Er	ppm	0.03	2.20	1.70	2.06	1.85	1.98	1.98	1.81	1.75	1.82	2.11
Tm	ppm	0.01	0.29	0.22	0.25	0.27	0.25	0.25	0.24	0.25	0.25	0.25
Yb	ppm	0.05	1.71	1.46	1.54	1.51	1.58	1.50	1.59	1.48	1.48	1.54
Lu	ppm	0.01	0.27	0.18	0.22	0.22	0.21	0.20	0.22	0.19	0.20	0.22
TOT/C	wt.%	0.02	0.05	0.05	0.08	0.06	0.05	0.05	0.03	0.08	0.05	0.04
TOT/S	wt.%	0.02	0.07	0.03	0.16	0.07	0.03	0.10	0.07	0.24	0.03	<0.02
Mg#			-	58.01	58.81	58.79	58.57	59.28	59.60	59.29	59.52	64.83

alkali silica (TAS) classification diagram (Le Bas et al., 1986), the rocks range from basanite to tephrite (Figure 4). The SiO_2 contents of the samples range from 44.89 to 48.26 wt.%.

According to the Nb/Y vs Zr/TiO_2 diagram (Winchester and Floyd, 1977), the samples plot in the field of basanite/nephelinite (Figure 5). Based on the La/ 10 – Y/ 15 – Nb/ 8
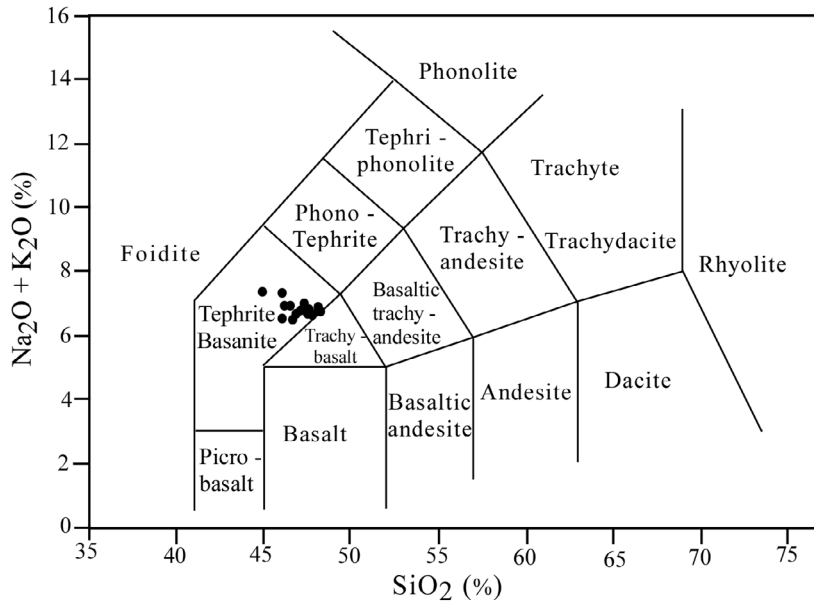
Figure 4. Classification of the Gandom Beryan basanitic rocks on the total alkali silica (TAS) plot (Le Bas et al., 1986).
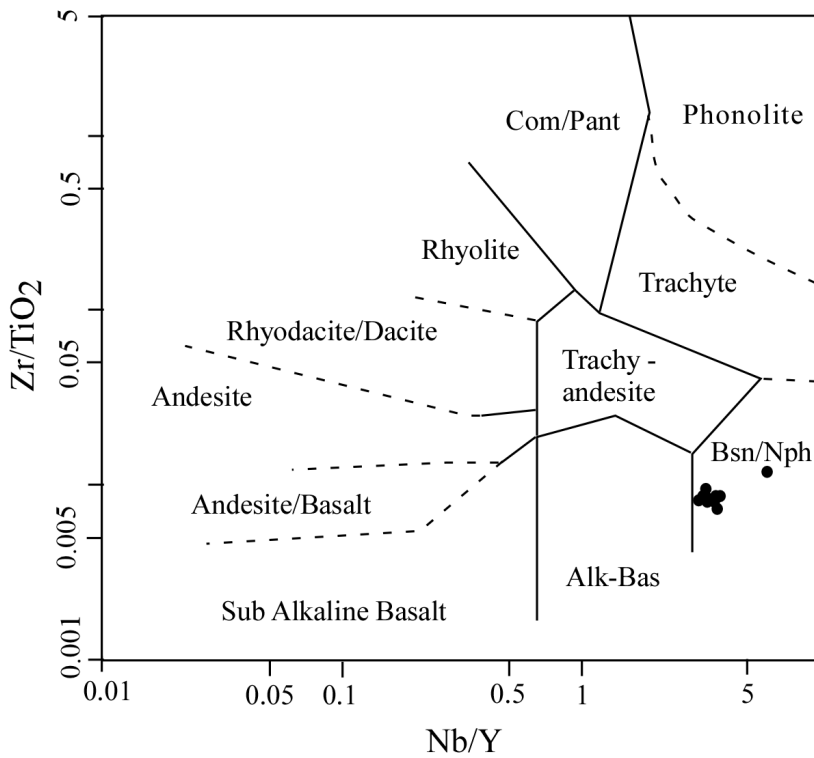
Figure 5. Nb/Y–Zr/TiO$_2$ plot (Winchester and Floyd, 1977) for the basic rocks of the Gandom Beryan area.

diagram (Cabanis and Lecolle, 1989), the rocks appear to be alkali basanites of the intercontinental rifts (Figure 6). The tectono-magmatic discrimination diagrams cannot often

show distinct different tectono-magmatic settings exactly, because they are established by old data (1970s–1980s) and their lines are often arbitrary, but they are frequently used
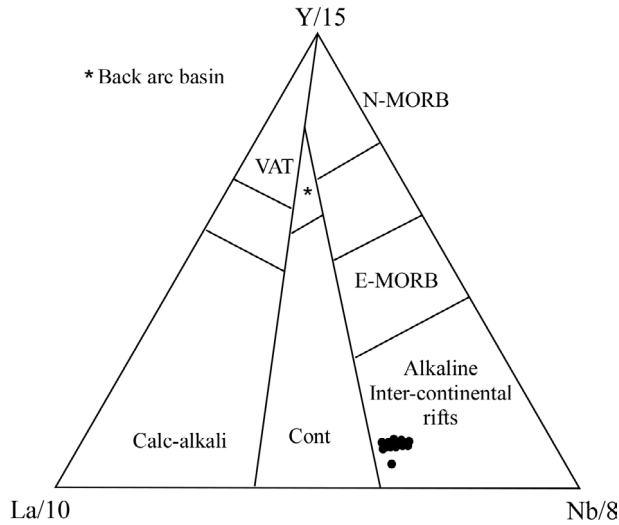
Figure 6. La/ 10–Y/ 15–Nb / 8 plot (Cabanis and Leocolle, 1989) for the Gandom Beryan rocks.

by petrologists, because they can show different tectonic environments just by the whole rock analyses.

CIPW normative calculations reveal that the studied alkali basanites are silica-undersaturated and contain up to 11.5 wt.% normative nepheline (Table 3). Compositionally, analyzed samples have low Fe/Mg ratios (Fe_2O_{3t}/MgO = 1.07–1.43) and low silica content with TiO_2 more than 2.28 wt.% and Ti/Y ratios of 601.92–813.61 suggest that they are high-Ti basalts (Peate et al., 1992; Marques et al., 1999). K_2O and Na_2O contents of the basanites vary between

2.08% and 2.82% and 3.84% and 5.04%, respectively. Thus it shows a sodic affinity of Gandom Beryan basanitic rocks. The samples have Mg# ranging from 58.01 to 64.83 (Table 2). The SiO_2 shows a negative correlation with MgO (7.72–10.29 wt.%), CaO (7.31–9.21 wt.%), Na_2O (3.84–5.04 wt.%), and P_2O_5 (0.81–1.43 wt.%), and a positive correlation with Al_2O_3 (12.78–13.71 wt.%), Fe_2O_3 (10.69–11.20 wt.%), K_2O (2.08–2.82 wt.%), and TiO_2 (2.30–2.81 wt.%) (Figure 7). The Ni (103–237 ppm), Sc (14–17 ppm), Sr (828.8–1610.6 ppm), Nb (68.9–142.6 ppm), and La

**Table 3.** CIPW normative calculation of the Gandom Beryan alkali basalts.

	Or	Ab	An	Ne	Di	Ol	Il	Hm	Tn	Pf	Ap	Sum
G1	12.824	24.519	8.792	8.17	18.385	7.974	0.321	10.74	0	3.714	2.061	97.498
G2	16.193	32.002	11.313	0.77	10.016	10.361	0.299	11	0	4.227	1.966	98.146
G3	13.77	29.938	11.035	2.851	12.991	9.534	0.321	10.79	0	3.782	2.108	97.12
G4	12.292	26.858	9.987	5.62	16.781	8.722	0.321	10.86	0	3.628	2.132	97.2
G5	15.188	25.963	10.561	4.821	15.404	9.221	0.321	11.04	0	3.697	2.226	98.442
G6	16.665	27.671	10.801	3.621	12.655	9.992	0.321	10.94	0	3.697	2.179	98.541
G7	15.897	30.684	10.054	2.447	11.5	9.984	0.299	10.88	0	4.192	1.919	97.855
G8	16.133	33.678	11.48	0	9.234	10.493	0.299	10.98	0.319	4.091	1.919	98.625
G9	14.42	27.91	9.461	5.141	13.23	9.491	0.321	10.84	0	3.748	2.179	96.741
G10	15.365	22.361	5.06	10.989	16.819	8.971	0.321	10.66	0	3.594	2.037	96.178
G11	20.329	29.735	9.963	7.591	7.433	3.572	0.278	9.94	0	4.348	2.795	95.984
G12	15.365	34.355	11.123	0	8.209	10.965	0.299	11.2	1.603	3.404	1.942	98.466
G13	13.71	30.878	10.28	3.533	12.82	9.31	0.299	10.71	0	4.022	2.013	97.577
G14	16.193	31.087	11.008	1.633	11.678	9.996	0.321	10.97	0	4.02	2.013	98.918
G15	16.429	31.397	11.77	0.594	10.845	10.057	0.299	10.9	0	4.073	2.013	98.377
G16	16.193	30.76	11.519	1.26	11.227	10.352	0.299	10.91	0	3.988	1.99	98.497
G17	13.829	30.766	9.464	4.144	12.661	10.042	0.321	10.89	0	3.884	2.108	98.11
G18	13.474	26.115	7.069	8.956	15.983	8.527	0.299	10.69	0	3.801	2.084	96.999
G19	16.488	28.664	10.932	2.12	11.807	10.18	0.321	10.82	0	3.833	2.155	97.321
G20	16.606	17.278	6.103	11.543	16.988	12.442	0.342	11.06	0	3.728	3.387	99.478
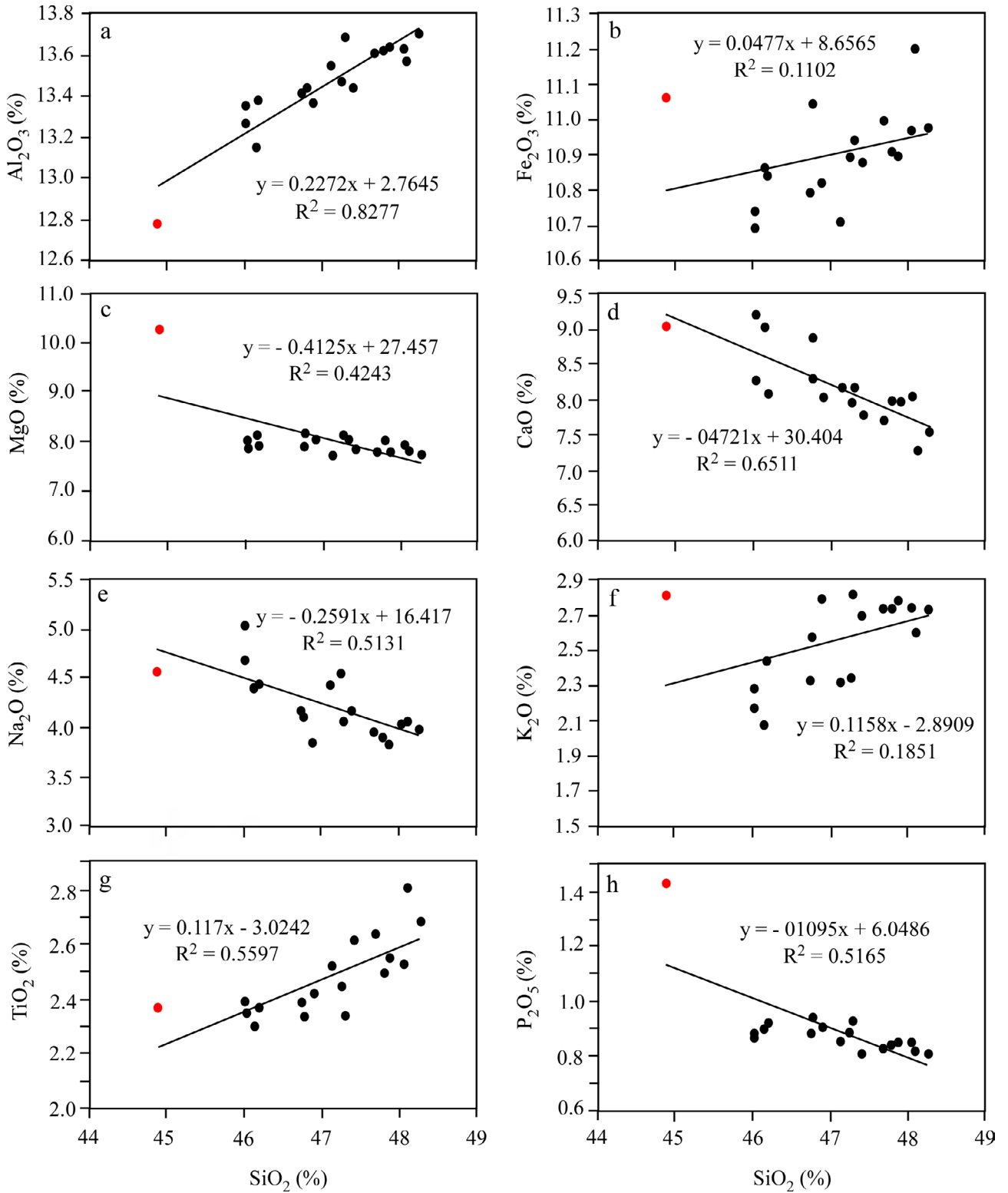
Figure 7. Variation diagrams of selected major elements versus SiO$_2$ for the Gandom Beryan basalts (the most primitive sample, G20 from the north of the area shown as red circle).

(40.5–96.8 ppm) concentrations of the basanites decrease with an increase in SiO_2 contents, while the V (157–185 ppm) concentrations increase with an increase in SiO_2 contents (Figures 8a–8f). Moreover, the Y (19.6–24.1 ppm) and Sm (7.02–11.62 ppm) contents do not show systematic trends versus Rb (25.7–51.9 ppm) (Figures 8g and 8h). Chemical data show that the sample G20 (shown as a red circle in Figures 7 and 8) is more primitive and it seems that the other samples (parental magmas) are derived from this primitive rock/melt.
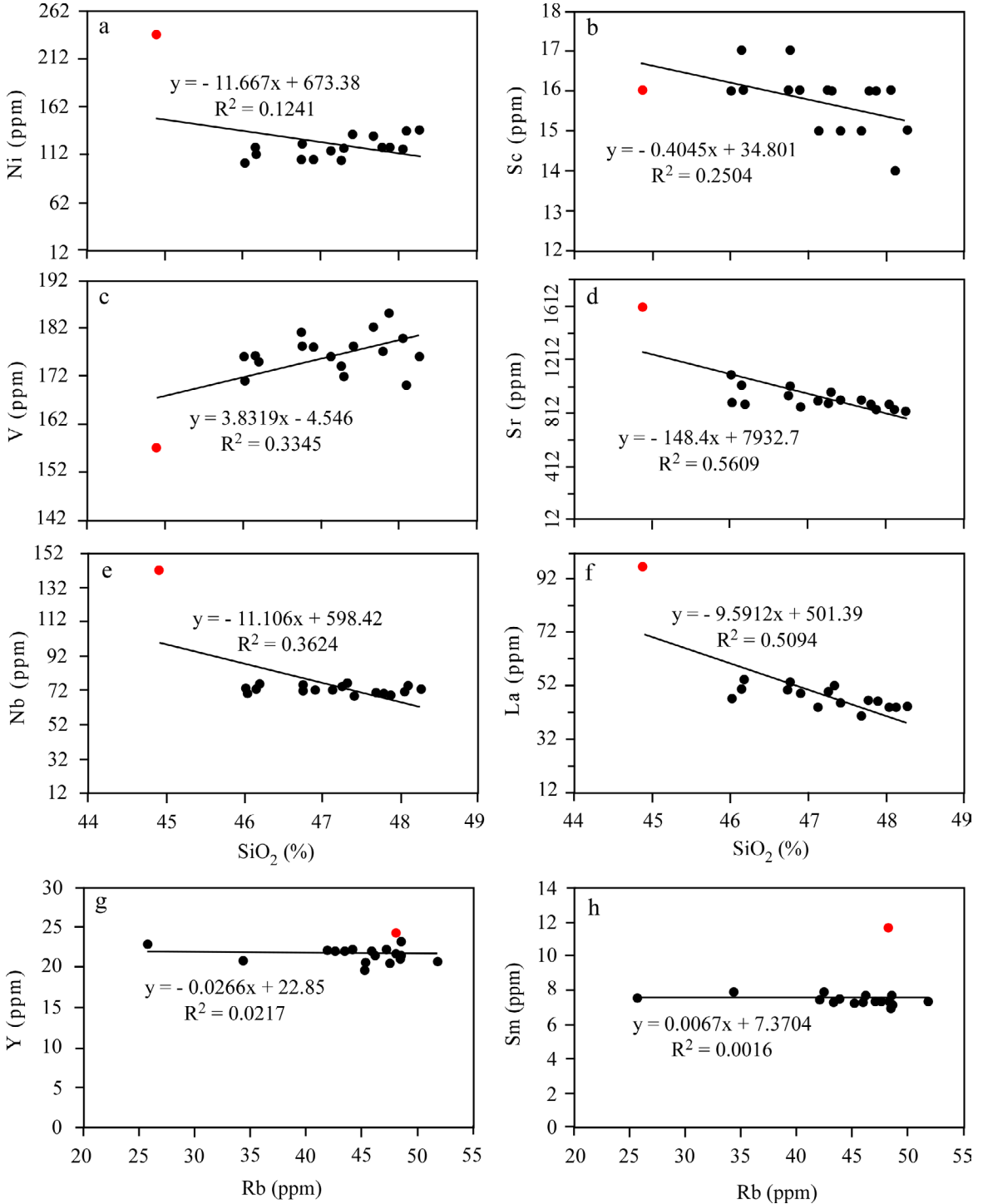
Figure 8. a–f) Variation diagrams of selected trace elements versus SiO_2 for the Gandom Beryan basalts, and g–h) Y and Sm versus Rb variation diagrams for the Gandom Beryan basalts (the most primitive sample, G20 from the north of the area shown as red circle).

Patterns of the basanites chondrite-normalized REE are shown in Figure 9. The samples are characterized by a significant enrichment of LREE with respect to chondrites ($[La/Yb]_N$ = 18.83–42.37). In comparison with the N-MORB (Gale et al., 2013), E-MORB (Gale et al., 2013), and OIB (Sun and McDonough, 1989), the Gandom Beryan rocks show an overall depletion in HREE such as Yb and Lu (Figure 9). With regard to the chondrite-normalized trace element plot (Figure 10), the Gandom Beryan rocks display an overall enrichment in highly incompatible elements as opposed to less incompatible ones. To make a meaningful comparison possible, the chondrite-normalized trace element diagrams of N-MORB, E-MORB, and OIB are shown in Figure 10. The Gandom Beryan was depleted in Zr, Hf, Ti, Y, and Yb with respect to OIB.

6.3. Strontium, neodymium, and lead isotopes

The whole-rock Sr, Nd, and Pb isotopic compositions for Gandom Beryan basanites are reported in Table 4 and shown by four isotopic correlation diagrams (Figures 11a–11d). The fields for depleted MORB mantle (DMM), enriched mantle (EM), bulk silicate earth (BSE), and mid-ocean ridge basalt (MORB) are indicated for comparison. The Gandom Beryan basanites display limited variation in isotopic compositions: $^{207}Pb/^{206}Pb$ = 0.826760–0.833880, $^{208}Pb/^{206}Pb$ = 2.066320–2.075730, $^{206}Pb/^{204}Pb$ = 18.725–18.891, $^{207}Pb/^{204}Pb$ = 15.613–15.620,

$^{208}Pb/^{204}Pb$ = 38.869–39.036, $^{143}Nd/^{144}Nd$ = 0.512676–0.512747 (εNd = 0.74 to 2.13), $^{87}Sr/^{86}Sr$ = 0.704291–0.705100. In the isotope correlation diagrams, the rocks plot in the field of Jeju Island alkali basalts (Park et al., 2005; Tatsumi et al., 2005; Chang et al., 2006; Choi et al., 2006; Brenna et al., 2012a, 2012b) between BSE and HIMU (high μ refers to high $^{238}U/^{204}U$) (Figures 11a–11d). However, the samples are depleted with respect to the bulk earth. According to the $^{143}Nd/^{144}Nd$ and $^{87}Sr/^{86}Sr$ ratios, Gandom Beryan rocks are similar to Pannonian basin Late Tertiary alkaline basalts (Salters et al., 1988; Embey-Isztin et al., 1993) (Figure 11a). In the Pb–Pb isotope diagram (Figure 11d), the basanitic rocks plot close to the field of enriched mantle II (EM-II) while the εNd(t) values are positive. As Pang et al. (2012) argued, the positive εNd(t) values and LREE enrichment of the Late Cenozoic intraplate alkali basalts in eastern Iran (Lut-Sistan region) represent an LREE-depleted mantle source. This source has been enriched from LREE and then melted to form the parent melts of Lut-Sistan alkali basalts (Pang et al., 2012). According to Pang et al. (2012), such enrichment that occurred in eastern Iran can be seen in the western Lut region due to exodus of melts or volatile-rich fluids released from the seismic low velocity region (Niu, 2008; Humphreys and Niu, 2009) or from the subsolidus peridotite just before melting (Zou and Zindler, 1996) into the asthenosphere.
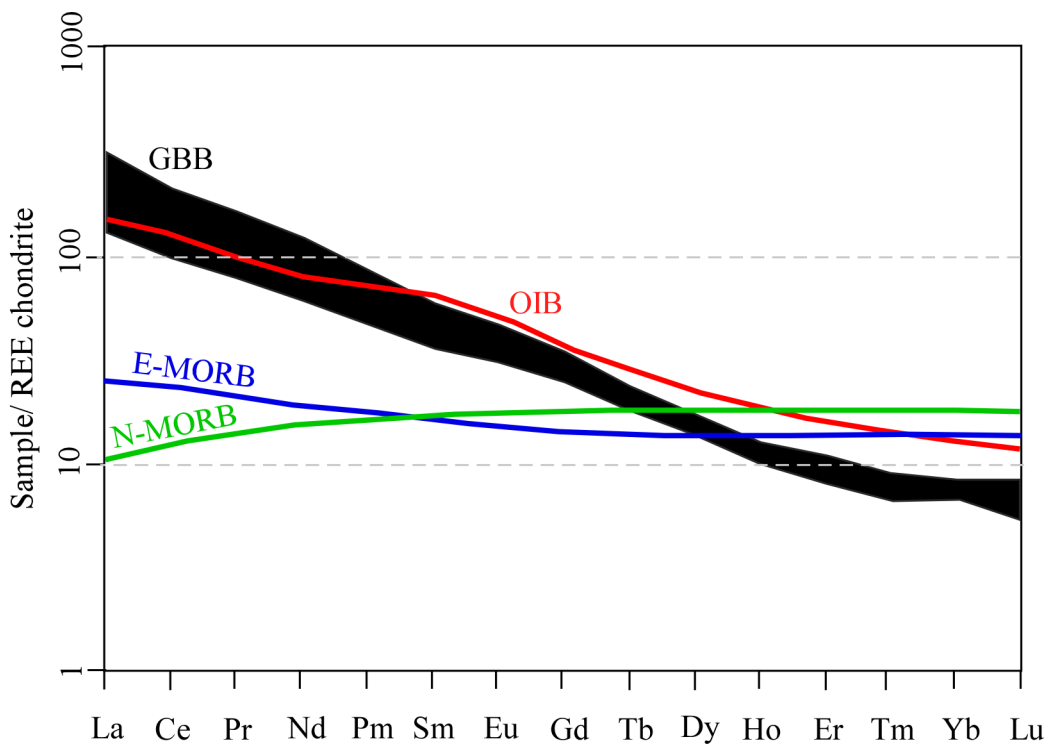
Figure 9. Chondrite-normalized (Boynton, 1984) rare earth elements patterns for basalts from the Gandom Beryan basanitic rocks.
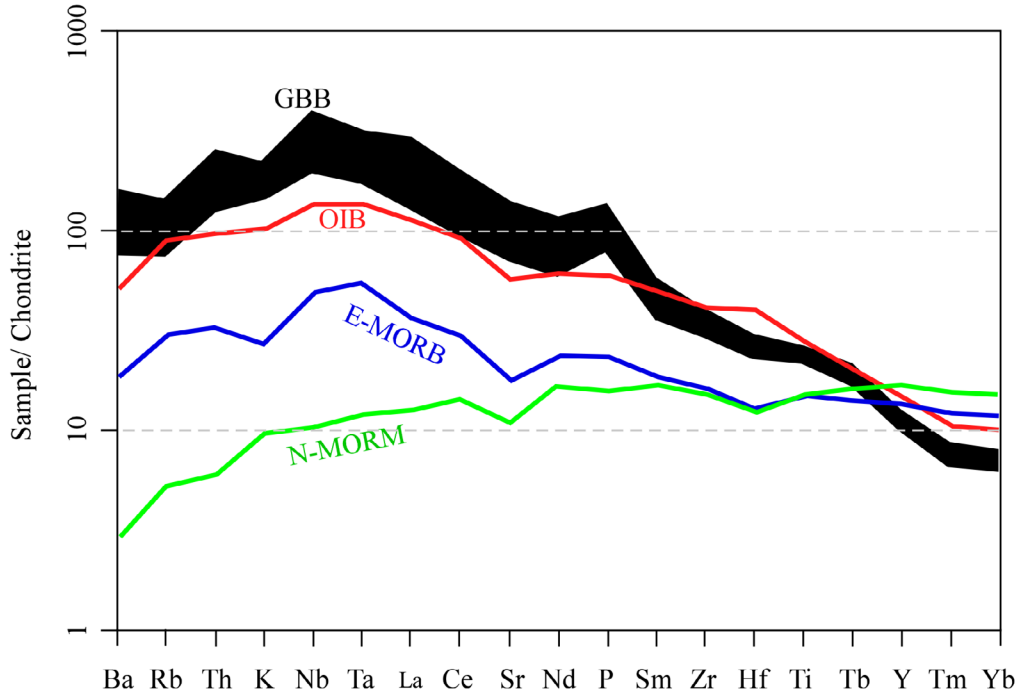
Figure 10. Chondrite normalized multi element distribution diagram for the Gandom Beryan Basalts (GBB) (normalization values are after Thompson, 1982).

Table 4. Sr-Nd-Pb isotope data for Gandom Beryan basanitic rocks.

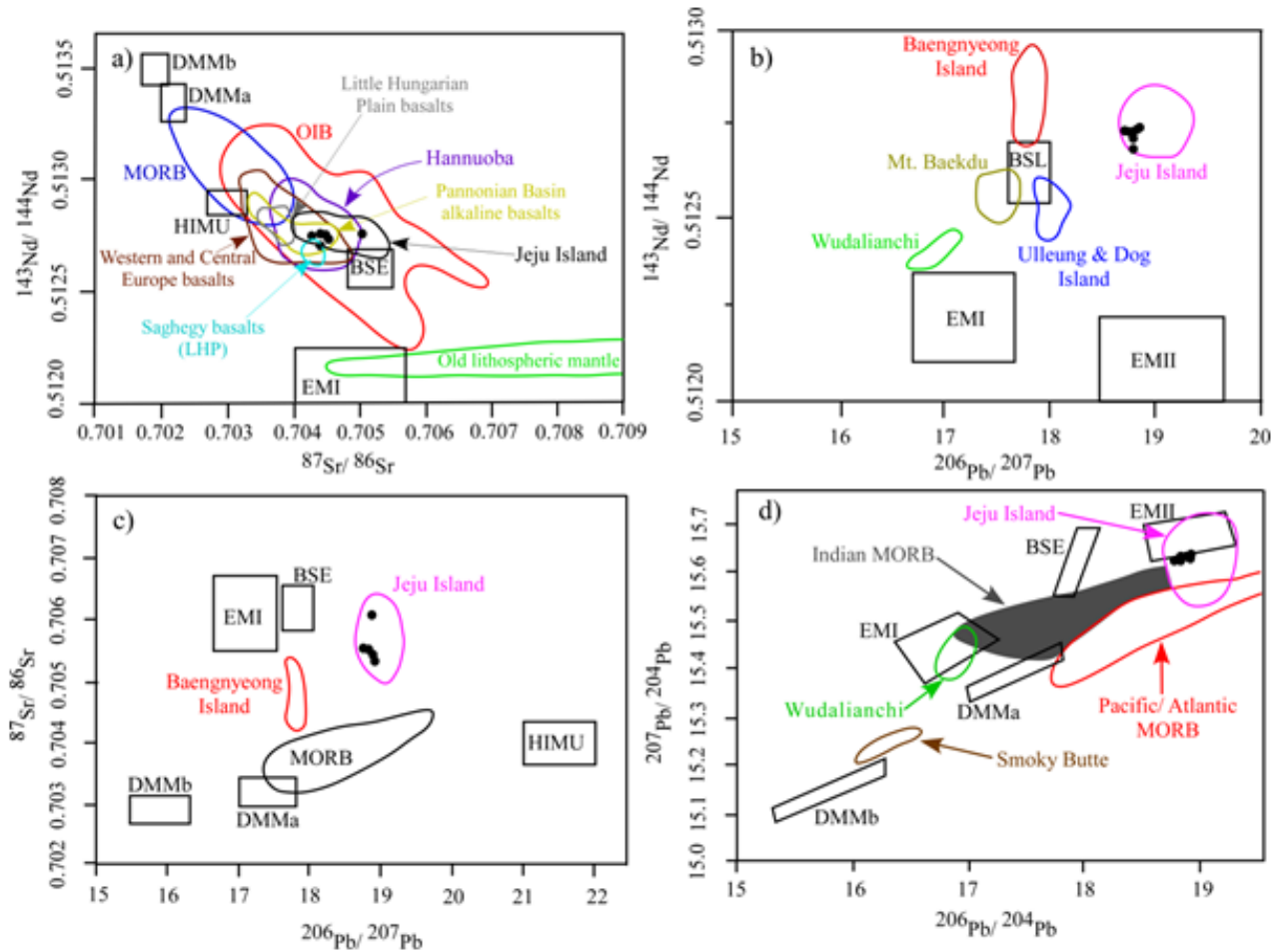| Sample	$^{87}Sr/^{86}Sr$	$^{143}Nd/^{144}Nd$	$^{206}Pb/^{204}Pb$	$^{207}Pb/^{204}Pb$	$^{208}Pb/^{204}Pb$	$^{208}Pb/^{206}Pb$	$^{207}Pb/^{206}Pb$	εNd
G20	0.704431	0.512676	18.834	15.620	39.003	2.070840	0.829350	0.740
G17	-	0.512747	18.891	15.619	39.036	2.066320	0.826760	2.130
G04	0.704567	0.512734	18.725	15.615	38.869	2.075730	0.833880	1.870
G13	0.704573	0.512725	18.841	15.617	38.968	2.068220	0.828860	1.700
G10	0.704291	0.512744	18.871	15.613	39.019	2.067630	0.827350	2.070
G01	0.705100	0.512743	18.862	15.617	39.000	2.067720	0.827980	2.050

7. Discussion

7.1. Crustal contamination and fractional crystallization

Crustal contamination is unavoidable during mantle-derived magma movement through the continental crust. Crustal contamination causes an increase in $^{87}Sr/^{86}Sr$ ratios and a decrease in $\varepsilon Nd(t)$. Due to the low $^{87}Sr/^{86}Sr$ ratios (0.704291–0.705100) and small $\varepsilon Nd(t)$ range (1.70 to 2.13), an intense assimilation of crustal rocks did not happen in Gandom Beryan basanites. We excluded the sample G20 (0.74), because it shows different isotopic characteristics possibly due to olivine and pyroxene bearing enclaves (Table 4). Therefore, crustal contamination processes can be excluded.

The Mg# of Gandom Beryan alkali basanites ranges from 58.01 to 64.83 that is lower than pristine mantle melts. The occurrence of clinopyroxene and olivine phenocrysts in the basanites is associated with crystal fractionation during the ascent of magma. Due to clinopyroxene and olivine fractionation, the trends of major and trace elements such as CaO, MgO, and Ni decrease while SiO_2 concentrations increase (Figures 7 and 8). The simultaneous increase in Fe_2O_3, TiO_2, and V as well as the increase in SiO_2 contents exhibits that the fractionation of Fe-Ti oxides was not significant (Figures 7 and 8). The concentration of Sm and Y (with high K_D for amphibole-liquid compared to pyroxene-liquid; Rollinson, 1993) versus Rb contents (index of fractionation) display that amphibole fractionation was not notable (Figure 8). Moreover, the lack of Eu anomalies exhibits the absence of plagioclase fractionation (Figure 9). Thus,

Figure 11. a) $^{87}Sr/ {}^{86}Sr$ versus $^{143}Nd/ {}^{144}Nd$, b) $^{206}Pb/ {}^{207}Pb$ versus $^{143}Nd/ {}^{144}Nd$, c) $^{206}Pb/ {}^{207}Pb$ versus $^{87}Sr/ {}^{86}Sr$, d) $^{206}Pb/ {}^{204}Pb$ versus $^{207}Pb/ {}^{204}Pb$ ratios for Gandom Beryan basalts. BSE = bulk silicate earth, fields of depleted MORB mantle (DMM), enriched mantle I (EMI), enriched mantle II (EMII) and HIMU (high μ, refers to high $^{238}U/{}^{204}U$) are after Rollinson (1993). Data sources: Little Hungarian Plain (LHP) (Harangi et al., 1995). Western and Central Europe (Wilson and Downes, 1991). Alkaline basalts from the Pannonian Basin (Embey-Isztin et al., 1993 and Salters et al., 1988). Saghegy basalts (LHP) (Harangi et al., 1995). MORB (mid ocean ridge basalts) and OIB (Zindler and Hart, 1986). Old lithospheric mantle (Zhang et al., 2002). The field of Jeju Island is after Tatsumi et al. (2005), Park et al. (2005), Choi et al. (2006), Chang et al. (2006), and Brenna et al. (2012a, 2012b). Data for Wudalianchi are after Zou et al. (2003). The field of Mt. Baekdu is after Basu et al. (1991) and Kuritani et al. (2009). Data for Baengnyeong Island are after Park and Park (1996), Kim et al. (2002), and Choi et al. (2006). The field of Ulleung and Dok Islands is after Tatsumoto and Nakamura (1991), Kim (2000), and Choi et al. (2006). Data for Indian MORB and Pacific and North Atlantic MORB are after Barry and Kent (1998) and Zou et al. (2000). The field of Smoky Butte is after Fraser et al. (1985).

the clinopyroxene and olivine are the main fractionation minerals in Gandom Beryan basanites.

7.2. Origin of Gandom Beryan rocks
According to Rollinson (1993) and Hauri et al. (1994), garnet is almost the only mineral phase in mantle that causes fractionation between middle REE (MREE) and heavy REE (HREE) of the alkali basalts. Thus the intense fractionation between MREE and HREE of the Gandom Beryan basanites exhibits residual garnet in the origin. Due to the fact that HREE concentrations in the studied basanites are less than those in the MORBs (Figure 9),

the parent magmas might have originated from the garnet stability mantle source, which is deeper than that of MORBs. In the alkali basalts, scandium contents indicate evidence for the low degree of melting, because this element is intensely partitioned into clinopyroxene and garnet mineral phases (Rollinson, 1993). Scandium concentrations range from 14 to 17 ppm in the Gandom Beryan alkali basanites, which are lower than Sc abundance of primitive MORB [ranging from 35 to 40 ppm, (Pearce et al., 1990)]. This indicates that the melting degrees were less than those necessary to produce MORB.

The high LaN/YbN (=18.83–42.37) ratios in the studied rocks suggest the important role played by clinopyroxene in the formation of such rocks because partition coefficients of HREE are higher than the LREE in clinopyroxene (Green, 1994). Furthermore, clinopyroxene is a major repository for REE during mantle melting and low pressure crystallization (Gaetani and Grove, 1995). According to Gallahan and Nielson (1992), the most important compositional factors controlling the REE partitioning between clinopyroxene and melt at constant temperature and pressure are the Ca content of the clinopyroxene and the Al content of the melt. Petrographic evidence indicates an abundance of clinopyroxene and apatite within the basanite samples. The sloping of rare earth elements (20.032 ≤ LaN/LuN ≤ 45.703) can be explained by the percentage of partial melting of mantle source. Moreover, the low abundance of HREE in basanitic rocks reflects the relation of these elements in residual garnet in the partially melted mantle. In addition, the studied basanite exhibits low Lu/Hf (0.0360–0.0510) and high LaN/YbN (=18.83–42.37). These chemical evidences show that the basaltic magma has been formed by melting of a mantle source with variable contents of residual garnet (Piccirillo and Melfi, 1988). HREE abundances are rather constant (Yb = 1.45–1.68 ppm), but LREE abundances are variable (La = 40.5–96.8 ppm). Thus there is a range in LaN/YbN = 18.83–42.37. These features are typical of alkaline magmas derived from a mantle peridotite source (Alibert et al., 1983).

The chondrite-normalized multielement distribution of the basanitic rocks from the Gandom Beryan area (Figure 10) shows significant enrichments of K, Nb, Ta, La, and Ce. All samples exhibit relative enrichment in high field strength elements (HFSE; La/Nb > 0.5) and do not display depletions in Nb as opposed to LILE (Sr and Ba). The dome-shape pattern is evident (Figure 10) and can be compared with the OIB-type basalts and may result from an undepleted source with low degree of partial melting. Moreover, all patterns show an overall relative enrichment with increasing incompatibility from right (Lu) toward left (Cs) on the plot with negative anomalies for Nd. The ratio of HFSE/LREE exhibits the origin of the lava in such a way that the ratios more than one suggest an asthenospheric origin (Smith et al., 1999). Thus, the high Nb/La ratios (1.355–1.750) of Gandom Beryan samples display an asthenospheric origin. The patterns for all rock types are almost parallel, implying their cogenetic nature. Isotopic data (Figure 11) on the studied rocks also indicate that they are similar to OIB-type basalt and are similar to those in Jeju Island. Finally, from geochemical, isotopic, and tectonic points of view, the Gandom Baryan basanite can be compared with the Kula alkaline volcanism in Turkey (Alıcı et al., 2002). According to Alıcı et al. (2002), the Kula basanitic rocks erupted in an extensional environment and represent a postcollisional magmatism during ascending of asthenospheric magmas. We suggest that the Gandom Baryan basanite suite is also originated in such a tectonic setting in the Central Iranian structural unit.

8. Conclusion

The Gandom Beryan Plio-Quaternary volcanic rocks are represented by high-Ti basanite. These rocks are alkali in nature and belong to intercontinental rifts related to alkali basanites. Generally, in these rocks, MgO versus major oxides and some trace elements diagrams display fractional crystallization of mafic minerals. Due to the fact that HREE concentrations in the studied basanites are less than those in the MORBs, the parent magmas might have originated from the garnet stability mantle source, which is deeper than those mentioned for MORBs.

The REE chondrite-normalized diagram displays a steep pattern representing the low-degree partial melting of mantle. In the chondrite-normalized trace elements spider plot, analyzed rocks display no enrichment in comparison with HFSE on the one hand and Ti, Ta, and Nb having no negative anomalies on the other hand. These features are related to magmas derived from the mantle source. The trace element and REE ratios indicate that the source of Gandom Beryan basanites was deep seated in the mantle.

According to Pb isotopes, Gandom Beryan volcanism was related to partial melting of enriched mantle that occurred within an extensional setting linked to the Nayband fault system.

Acknowledgments

References

Aldanmaz E, Köprübaşı N, Gürer ÖF, Kaymakçi N, Gourgaud A (2006). Geochemical constraints on the Cenozoic, OIB-type alkaline volcanic rocks of NW Turkey: implications for mantle sources and melting processes. Lithos 86: 50-76.

Alibert C, Michard A, Albarede F (1983). The transition from alkali basalts to kimberlites: isotopic and trace element evidence from melilitites. Contrib Mineral Petrol 82: 176-186.

Alıcı P, Temel A, Gourgaud A (2002). Pb-Nd-Sr isotope and trace element geochemistry of Quaternary extension-related alkaline volcanism: a case study of Kula region (western Anatolia, Turkey). J Volcanol Geoth Res 115: 487-510.

Barry TL, Kent RW (1998). Cenozoic magmatism in Mongolia and the origin of Central and East Asian basalts. In: Flower MFJ, Chung SL, Lo CH, Lee TY, editors. Mantle Dynamics and Plate Interactions in East Asia. Geodynamics Series 27. AGU, Washington, pp. 347-364.

Basu AR, Wang JW, Huang WK, Xie GH, Tatsumoto M (1991). Major element, REE, and Pb, Nd and Sr isotopic geochemistry of Cenozoic volcanic rocks of eastern China: implications for their origin from suboceanic-type mantle reservoirs. Earth Planet Sci Lett 105: 149-169.

Berberian M, King GCP (1981). Towards a paleogeography and tectonic evolution of Iran. Can J Earth Sci 18: 210-265.

Boynton WV (1984). Cosmochemistry of the rare earth elements: meteorite studies. In: Henderson P, editor. Rare Earth Element Geochemistry. Amsterdam, the Netherlands: Elsevier, pp. 63-107.

Brenna M, Cronin SJ, Smith IEM, Maas R, Sohn YK (2012a). How small-volume basaltic magmatic systems develop: a case study from the Jeju Island Volcanic Field, Korea. J Petrol 53: 985-1018.

Brenna M, Cronin SJ, Smith IEM, Sohn YK, Maas R (2012b). Spatio-temporal evolution of a dispersed magmatic system and its implications for volcano growth, Jeju Island Volcanic Field, Korea. Lithos 148: 337-352.

Cabanis B, Lecolle M (1989). Le diagramme La/10-Y/15-Nb/8: un outil pour la discrimination des series volcaniques et la mise evidence des proccessus de mélange et/ou de contamination crustale. C.R. Academic Sci Seri II 309: 2023-2029 (in French).

Camp VE, Griffis RJ (1982). Character, genesis and tectonic setting of igneous rocks in the Sistan suture zone, eastern Iran. Lithos 15: 221-239.

Carlson RW, Lugmair GW, Macdougall JD (1981). Columbia River volcanism: the question of mantle heterogeneity or crustal contamination. Geochim Cosmochim Ac 45: 2483-2499.

Chang KH, Park JB, Kwon ST (2006). Geochemical characteristics of trachytes in Jeju Island. J Geol Soc Korea 42: 235-252.

Choi SH, Mukasa SB, Kwon ST, Andronikov AV (2006). Sr, Nd, Pb and Hf isotopic compositions of late Cenozoic alkali basalts in South Korea: evidence for mixing between the two dominant asthenospheric mantle domains beneath East Asia. Chem Geol 232: 134-151.

Embey-Isztin A, Downes H, James DE, Upton BGJ, Dobosi G, Ingram GA, Harmon RS, Scharbert HG (1993). The petrogenesis of Pliocene alkaline volcanic rocks from the Pannonian Basin, Eastern Central Europe. J Petrol 34: 317-343.

Esmaiely D, Nédélec A, Valizadeh MV, Moore F, Cotton J (2005). Petrology of the Jurrasic Shah-Kuh granite (eastern Iran), with reference to tin mineralization. J Asian Earth Sci 25: 961-980.

Fraser KJ, Hawkesworth CJ, Erland AJ, Mitchell RH, Scott-Smith BH (1985). Sr, Nd and Pb isotope and minor element geochemistry of lamproites and kimberlites. Earth Planet Sci Lett 76: 57-70.

Gaetani GA, Grove TL (1995). Partitioning of rare earth elements between clinopyroxene and silicate melt crystal-chemical controls. Geochim Cosmochim Ac 59: 1951-1962.

Gale A, Dalton CA, Langmuir CH, Su Y, Schilling J (2013). The mean composition of ocean ridge basalts. Geochem Geophy Geosy 14: 489-518.

Gallahan WE, Nielson RL (1992). The partitioning of Sc, Y, and the rare earth elements between high-Ca pyroxene and natural mafic to intermediate lavas at 1 atmosphere. Geochim Cosmochim Ac 56: 2387-2404.

Green TH (1994). Experimental study of trace element partitioning applicable to igneous petrogenesis-Sedona 16 years later. Chem Geol 117: 1-36.

Harangi S, Vaselli O, Tonarini S, Szabó CS, Harangi R, Coradossi N (1995). Petrogenesis of Neogene extension-related alkaline volcanic rocks of the Little Hungarian Plain volcanic field (Western Hungary). In: Downes H, Vaselli, O, editors. Neogene and related magmatism in the Carpatho-Pannonian Region: Acta Vulcanologica, 7. pp. 173-187.

Hauri EH, Wagner TP, Grove TL (1994). Experimental and natural partitioning of Th, U, Pb and other trace elements between garnet, clinopyroxene and basaltic melts. Chem Geol 117: 149-166.

Hawkesworth CJ, Gallager K, Kelley S, Mantovani MSM, Peate D, Regelous M, Rogers N (1992). Paraná magmatism and the opening of the South Atlantic. In: Storey B, Alabaster A, Pankhurst R, editors. Magmatism and the Causes of Continental Break-up. Geol Soc Spec Publ 68. pp. 221-240.

Hofmann AW, Jochum KP, Seufert M, White WM (1986). Nb and Pb in oceanic basalts: new constraints on mantle evolution. Earth Planet Sc Lett 79: 33-45.

Humphreys ER, Niu Y (2009). On the composition of ocean island basalts (OIB): the effects of lithospheric thickness variation and mantle metasomatism. Lithos 112: 118-136.

Kim KH (2000). K-Ar ages and Nd–Sr isotopes of Dokdo alkali volcanic rocks in the East Sea, South Korea. J Geol Soc Korea 36: 313-324.

Kim KH, Keisuke N, Jang HS, Hirochika S, Chung JI (2002). Nd, Sr and noble gas isotopic compositions of alkali basaltic rocks and mantle xenoliths in the Baegryongdo. Econ Environ Geol 35: 523-532.

Kluyver HM, Griffis RJ, Alavi-Naini M, Chance PN, Meixner HM, Tirrul R (1981). Geological map of Lakar Kuh-1/250000, Sheet 7453. Geological survey of Iran.

Koszowska E, Wolska A, Zuchiewicz W, Cuong NQ, Pécskay Z, (2007). Crustal contamination of Late Neogene basalts in the Dien Bien Phu Basin, NW Vietnam: some insights from petrological and geochronological studies. J Asian Earth Sci 29: 1-17.

Kuritani T, Kimura JI, Miyamoto T, Wei H, Shimano T, Maeno F, Jin X, Taniguchi H (2009). Intraplate magmatism related to deceleration of upwelling asthenospheric mantle: implications from the Changbaishan shield basalts, northeast China. Lithos 112: 247-258.

Le Bas MJ, Le Maitre RW, Streckeisen A, Zanettin B (1986). A chemical classification of volcanic rocks based on the total alkali–silica diagram. J Petrol 27: 745-750.

Ma GSK, Malpas J, Xenophontos C, Suzuki K, Lo CH (2011b). Early Cretaceous volcanism of the Coastal Ranges, NW Syria: magma genesis and regional dynamics. Lithos 126: 290-306.

MacKenzie WS, Donaldson CH, Guilford C (1982). Atlas of Igneous Rocks and Their Textures. New York, NY, USA: Wiley.

Mahoney JJ (1988). Deccan traps. In: Macdougall JD, editor. Continental Flood Basalts. Dordrecht, Netherlands: Kluwer, pp. 151-194.

Marques LS, Dupré B, Piccirillo EM (1999). Mantle source compositions of the Paraná Magmatic Province (southern Brazil): evidence from trace element and Sr–Nd–Pb isotope geochemistry. J Geodyn 28: 439-458.

Meibom A, Anderson DL (2003). The statistical upper mantle assemblage. Earth Planet Sc Lett 217: 123-139.

Nabavi MH (1976). History of Iran Geology. Geological Survey and Mineral Exploration Country.

Niu YL (2008). The origin of alkaline lavas. Science 320: 883-884.

O'Reilly SY, Zhang M (1995). Geochemical characteristics of lava-field basalts from eastern Australia and inferred sources: connections with the subcontinental lithospheric mantle. Contrib Mineral Petr 121: 148-170.

Pang KN, Chung SL, Zarrinkoub MH, Mohammadi SS, Yang HM, Chu CH, Lee HY, Lo CH (2012). Age, geochemical characteristics and petrogenesis of Late Cenozoic intraplate alkali basalts in the Lut–Sistan region, eastern Iran. Chem Geol 306: 40-53.

Park JB, Park KH (1996). Petrology and petrogenesis of the Cenozoic alkali volcanic rocks in the middle part of Korean peninsula (I): petrography, mineral chemistry and whole rock major element chemistry. J Geol Soc Korea 32: 223-249.

Park KH, Park JB, Cheong CS, Oh CW (2005). Sr, Nd and Pb isotopic systematics of the Cenozoic basalts of the Korean Peninsula and their implications for the Permo-Triassic continental collision boundary. Gondwana Res 8: 529-538.

Pearce JA, Bender JF, De Long SE, Kidd WSF, Low PJ, Güner Y, Saroglu F, Yilmaz Y, Moorbath S, Mitchell JG (1990). Genesis of collision volcanism in Eastern Anatolia, Turkey. J Volcanol Geoth Res 44: 189-229.

Peate DW, Hawkesworth CJ, Mantovani SM (1992). Chemical stratigraphy of the Paraná lavas (South America): classification of magma types and their spatial distribution. B Volcanol 55: 119-139.

Peters TJ, Menzies M, Thirwall M, Kyle PR (2008). Zuni-Bandera volcanism, Rio Grande, USA-Melt formation in garnet and spinel-facies mantle straddling the asthenosphere-lithosphere boundary. Lithos 102: 295-315.

Piccirillo EM, Melfi AJ (1988). The Mesozoic flood volcanism of the Paraná Basin: Petrogenetic and Geophysical Aspects. Universidade de São Paulo, São Paulo.

Raeisi D (2011). Geochemistry and petrogenesis of Gandom Beryan Quaternary lava flowed, north of Shahdad-Kerman: along with crystal size distribution and remote sensing studies, MSc, Shahid Bahonar University, Kerman. Iran.

Rocha-Júnior ERVR, Marques LS, Babinski M, Nardy AJR, Figueiredo AMG, Machado FB (2013). Sr-Nd-Pb isotopic constraints on the nature of the mantle sources involved in the genesis of the high-Ti tholeiites from northern Paraná Continental Flood Basalts (Brazil). J S Am Earth Sci 46: 9-25.

Rollinson HR (1993). Using Geochemical Data: Evaluation, Presentation and Interpretation. Singapore: Longman.

Saadat S, Karimpour MH, Stern Ch (2010). Petrochemical characteristics of neogene and quaternary alkali olivine basalts from the western margin of the Lut Block, Eastern Iran. Iran J Earth Sci 2: 87-106.

Salters VJM, Hart SR, Panto G (1988). Origin of late Cenozoic volcanic rocks of the Carpathian arc, Hungary. In: Royden LH, Horvath F, editors. The Pannonian Basin; a Study in Basin Evolution. Am Assoc of Petr Geol M 45. pp. 279-292.

Samani B, Zhuyi C, Xuetao G, Chuan T (1994). Geochemistry of Quaternary olivine basalts from the Lut Block, eastern Iran. Geol Q 3: 40-63.

Smith EI, Sánchez A, Walker JD, Wang K (1999). Geochemistry of mafic magmas in the Hurricane Volcanic Field, Utah: implications for small- and large-scale chemical variability of the lithospheric mantle. J Geol 107: 433-448.

Späth A, Le Roex AP, Opiyo-Akech N (2001). Plume-lithosphere interaction and the origin of continental rift-related alkaline volcanism-the Chyulu Hills Volcanic Province, southern Kenya. J Petrol 42: 765-787.

Stöcklin E, Eftekharnejad G, Hoshmandzadeh A (1971). Initial investigation of central Lut block, eastern Iran, Report No. 22, Geological survey of Iran.

Sun SS, McDonough WF (1989). Chemical and isotopic systematics of ocean basalt: implications for mantle composition and processes. In: Saunders AD, Norry M, editors. Magmatism in the Ocean Basins. Geol Soc Spec Publ 42. pp. 323-345.

Tang YJ, Zhang HF, Ying JF (2006). Asthenosphere–lithospheric mantle interaction in an extensional regime: implication from the geochemistry of Cenozoic basalts from Taihang Mountains, North China Craton. Chem Geol 233: 309-327.

Tatsumi Y, Shukuno H, Yoshikawa M, Chang Q, Sato K, Lee MW (2005). The petrology and geochemistry of volcanic rocks on Jeju Island: plume magmatism along the Asian continental margin. J Petrol 46: 523-553.

Tatsumoto M, Nakamura Y (1991). DUPAL anomaly in the Sea of Japan: Pb, Nd, and Sr isotopic variations at the eastern Eurasian continental margin. Geochim Cosmochim Acta 55: 3697-3708.

Taylor SR, McLennan SM (1995). The geochemical evolution of the continental crust. Rev Geophys 33: 241-265.

Thompson RN (1982). Magmatism of the British Tertiary province Scottish. J Geol 18: 49-107.

Walker RT, Gans P, Allen MB, Jackson J, Khatib M, Marsh N, Zarrinkoub M (2009). Late Cenozoic volcanism and rates of active faulting in eastern Iran. Geophys J Int 177: 783-805.

Walker R, Jackson J (2002). Offset and evolution of the Gowk fault, S.E. Iran: a major intra-continental strike-slip system. J Struct Geol 24: 1677-1698.

Weinstein Y, Navon O, Altherr R, Stein M (2006). The role of lithospheric mantle heterogeneity in the generation of Plio–Pleistocene alkali basaltic suites from NW Harrat Ash Shaam. J Petrol 47: 1017-1050.

Wilson M, Downes H (1991). Tertiary-Quaternary extension-related alkaline magmatism in Western and Central Europe. J Petrol 32: 811-849.

Winchester JA, Floyd PA (1977). Geochemical discrimination of different magma series and their differentiation products using immobile elements. Chem Geol 20: 325-343.

Xu YG, Ma JL, Frey FA, Feigenson MD, Liu JF (2005). Role of lithosphere–asthenosphere interaction in the genesis of Quaternary alkali and tholeiitic basalts from Datong, western North China Craton. Chem Geol 224: 247-271.

Zhang HF, Sun M, Zhou XH, Fan WM, Zai MG, Ying JF (2002). Mesozoic lithosphere destruction beneath the North China Craton: evidence from major-, trace-element and Sr-Nd-Pb isotope studies of Fangcheng basalts. Contrib Mineral Petrol 144: 241-253.

Zindler A, Hart S (1986). Chemical geodynamics. Annu Rev Earth Planet Sci 14: 493-571.

Zou H, Reid MR, Liu Y, Yao Y, Xu X, Fan Q (2003). Constraints on the origin of historic potassic basalts from northeast China by U–Th disequilibrium data. Chem Geol 200: 189-201.

Zou H, Zindler A (1996). Constraints on the degree of dynamic partial melting and source composition using concentration ratios in magmas. Geochim Cosmochim Ac 60: 711-717.

Zou HB, Zindler A, Xu XS, Qi Q (2000). Major, trace element, and Nd, Sr and Pb isotope studies of Cenozoic basalts in SE China: mantle sources, regional variations, and tectonic significance. Chem Geol 171: 33-47.